Mathematical Biosciences and Engineering

https://www.aimspress.com/journal/mbe

MBE, 23(5): 1315–1339.
DOI: 10.3934/mbe.2026048
Received: 31 July 2025
Revised: 19 February 2026
Accepted: 18 March 2026
Published: 02 April 2026

Research article

Imitation dynamics in vaccination under partial and temporary immune protection

Paulo Doutor[1,2,*], **Ricardo Castelhano**[1], **Maria do Céu Soares**[1,2], **Bob Kooi**[3,4] **and Paula Patricio**[1,2]

[1] Center for Mathematics and Applications (NOVA Math), NOVA FCT, Caparica, 2829-516, Portugal

[2] Department of Mathematics, NOVA FCT, Caparica, 2829-516, Portugal

[3] Faculty of Science, Vrije Universiteit, Amsterdam, The Netherlands

[4] BCAM - Basque Center for Applied Mathematics, Bilbao, Spain

* **Correspondence:** Email: pjd@fct.unl.pt; Tel: +351-212-948-300.

Abstract: Vaccination has been the most effective strategy to contain and control infectious disease epidemics. Over the past decades, its success and the consequent herd immunity changed public perceptions on the disease and vaccination's expected costs which, in some cases, resulted in vaccine hesitancy. This work extends the classical SIR model by incorporating both temporary and partial immunity, along with individual vaccination decisions driven by an imitation dynamics approach based on perceived expected costs. Our methodology relied on the stability analysis of the equilibria and the investigation of bifurcation phenomena within the model. To this end, we employed classical local asymptotic techniques, complemented by numerical continuation methods and the computation of Lyapunov exponents. The analysis of the model revealed an interplay between incomplete immune protection and imitation parameters, with rich dynamics involving oscillatory and chaotic behavior for low waning immunity rates and/or high protection against reinfection, and for high social-learning rate. Furthermore, exploring temporary immunity led to the conclusion that for diseases with shorter immunity periods and for vaccines with high relative expected cost, people will rapidly decline any vaccination efforts. These findings emphasize the importance of human behavior for a population in an epidemic landscape, and may provide insight on how to adapt and improve public health interventions.

Keywords: Epidemiological models; suboptimal immunity; vaccination strategies; imitation dynamics; complex dynamics; Lyapunov exponents; bifurcation analysis

1. Introduction

The recent pandemic of the coronavirus disease (COVID-19), caused by the coronavirus SARS-CoV-2, was a reminder of how hindering infectious diseases can be to society, with around 7.1 million deaths being registered since the outbreak's onset [1]. It highlighted vaccination as one of the most crucial strategies for containing epidemics, while drawing attention to its vulnerability to public opinion and the population's adherence. Social dynamics – such as public fears about vaccine safety and the given opportunity of individuals to rely on others' immunity to get protection (free-riding) – have consistently interfered with achieving the high immunization coverage needed for elimination since vaccines became widely availabl (see Bauch et al. [2], Oraby et al. [3], Funk et al. [4], Bauch and Galvani [5], Ibuka et al. [6], and Wagner et al. [7]). As a result, public health strategies primarily aim at controlling the spread of disease and achieving regional elimination rather than global eradication [8].

Game theory integrated into mathematical modeling of epidemic dynamics [9, 10] has become a common approach to describe how decisions, given different intervention possibilities, may vary over time. One of the most widely explored uses of game theory in this framework involves voluntary vaccination (see the works of Bauch and Earn [11], Reluga et al. [12], Xu and Cressman [13], and Chalub et al. [14]), where individuals are assumed to be fully rational and capable of evaluating the risks and benefits of vaccination accurately. We model this behavior using payoff functions derived from quantities established in the epidemiological models. Based on their perceived expected costs they decide whether or not to vaccinate. These individual choices, in turn, influence the overall vaccination rate within the model. The analysis seeks to determine the broad vaccination strategy at which no player can gain a better payoff by changing their decision—a state known as the Nash equilibrium.

A mathematical modeling framework that incorporates human choices via payoff functions is known as imitation dynamics, which describes how individuals' strategies evolve by observing and replicating patterns of action that have been more successful. When considering a heterogeneous population, individuals can adapt their behavior by learning from others, provided that there is an increase in payoff. This modeling of human behavior has already been applied to various scenarios such as vaccination (see, for example, the works of Bauch [15], Bauch and Bhattacharyya [16], Onofrio et al. [17], Feng and Wang [18], and Ndii et al. [19]), pediatric infectious diseases [20], and the COVID-19 pandemic [21].

To develop an imitation-based approach when considering a generic population, we must consider the rate of change of each compartment in the epidemiological model to be dependent on the strategy distribution across the entirety of the population, similar to an evolutionary game approach [22]. Specifically, if we take x as the fraction of the population adopting strategy A, the rate of change of x is given by

$$x'(t) = kx(1 - x)\Delta E,$$

where k is the social-learning rate and $\Delta E = E(A) - E(B)$ is the payoff difference, with $E(A)$ and $E(B)$ representing the payoffs for strategies A and B, respectively.

Payoff functions are used to strike a balance between perceived expected costs of vaccination and infection, which in turn can be defined based on epidemic factors. For example, D'Onofrio et al. [17] accounted for vaccine side effects by defining the perceived vaccination payoff as $E(A) = -\alpha x(t)$, where α is the per-capita probability of a vaccine side effect per dose. This translates to $E(A)$ being proportional to x, since perception of vaccination side effects tends to increase as more people get vac-

cinated. On the other hand, Bauch [15] assumed the perceived payoff of vaccination to be constant and the perceived payoff of infection to be proportional to the disease prevalence. Despite varying assumptions, most imitation-based vaccination game models reach a similar conclusion: when individuals act purely out of self-interest, vaccination rates fall short of what's needed for herd immunity. Even with a perfect vaccine, widespread immunization tends to drive disease incidence so low that people no longer feel motivated to get vaccinated. In [23], d'Onofrio et al. explore how even small public incentives can help sustain vaccination levels high enough to eliminate disease. Generally, these models predict three possible outcomes depending on transmission and perceived benefits: (1) no disease and no vaccination when the infection is not easily spread, (2) persistent infection without vaccination when vaccine benefits are perceived as low, and (3) a stable but imperfect vaccination level with ongoing disease. The last scenario may involve oscillations in both disease and vaccination rates, influenced by how quickly individuals adapt their behavior in response to others [15, 17].

Partial and/or temporary immunity also plays a fundamental role in shaping the dynamics of infectious disease transmission. Many infections and vaccines - especially those caused by rapidly evolving pathogens - provide only partial or temporary immunity. This incomplete protection allows for breakthrough infections and recurrent outbreaks, which can sustain transmission even in highly vaccinated populations. As a result, accurately representing induced immunity in mathematical models is essential to understand and predict long-term epidemic behavior, assess control strategies, and guide public health decisions for a wide range of infectious diseases.

Taylor et al. [24] had already shown that a loss of immunity through reinfection led to periodic outbreaks that acquired pulsating characteristics as more people got reinfected. Furthermore, Chen et al. [25] studied an imitation-driven mathematical model with imperfect vaccination, where they found that the system could fall into a hysteresis loop with rises and drops of the vaccination level, as long as a specific window of perceived vaccination risk and vaccine efficacy was maintained. This is akin to what was shown in Doutor et al.'s work [26], where specific parameter combinations could push the system into behaving periodically when crossing the Hopf bifurcation threshold. However, and conversely to the model in Doutor et al model [26], in which irregular oscillations were detected, Chen et al. [25] did not report any chaotic behavior in their model.

With this in mind, key aspects of interest for these models include the potential for destabilization through periodic behavior and chaotic dynamics and the sensitivity of the Hopf bifurcation to immunity-related parameters.

In this work, we introduce an extension of Doutor's [26] standard SIR model that incorporates partial and temporary immunity and also individual vaccination decisions ruled by an imitation-driven strategy, where payoffs are symmetric to the expected costs of each strategy: vaccinating and non-vaccinating. The expected cost of vaccination, representing the individuals' perception of vaccine-related adverse events and other costs due to vaccination, is assumed to be constant, while the expected cost of non-vaccination accounts for the perception of serious disease following infection, as described by Reluga et al. [12]. The fraction of individuals choosing to vaccinate is reflected by the vaccination rate at birth in the epidemic model. The resulting model shows important deviations from the behavior previously observed in the model with complete immunity in [26].

This paper is organized as follows. We begin by presenting the full mathematical model, including a detailed mathematical analysis. We then evaluate the complex behavior of the system, focusing on scenarios highlighting the interplay between social learning and the perceived relative cost of vaccina-

tion. Lastly, we explore the impact of temporary immunity, to underline the conditions under which instability and oscillations may arise.

2. The SIRISp model with imitation dynamics

We start with the standard SIR model, where we introduce temporary immunity, as a transition from the recovered class to the susceptible class at a waning rate $\bar{\alpha}$ yrs^{-1}. We also introduce partial immunity by allowing the recovered individuals to be reinfected at a reduced rate $\sigma\beta$, where σ varies between 0 and 1. The model is described by the following system of equations

$$\begin{cases} \dfrac{dS}{dT} = \mu N - \dfrac{\beta IS}{N} - \mu S + \bar{\alpha} R \\ \dfrac{dI}{dT} = \dfrac{\beta IS}{N} + \dfrac{\sigma\beta IR}{N} - (\tau + \mu) I \\ \dfrac{dR}{dT} = \tau I - \dfrac{\sigma\beta IR}{N} - (\mu + \bar{\alpha}) R \end{cases} \tag{2.1}$$

where μ is the birth and death rate in yrs^{-1}, τ is the recovery rate in yrs^{-1}, and β is the transmission rate; see Table 1. The basic reproduction number of this model is $R_0 = \frac{\beta}{\tau+\mu}$. The total population is constant, so we assume $N = 1$ and interpret S, I, and R as proportions of the population.

Table 1. Parameters used in the SIRIS Model 2.1.

Parameters	Description	Values
μ	birth/death rate	$\frac{1}{35}$ yrs^{-1}
τ	recovery rate	1 yrs^{-1}
σ	partial immunity reduction factor	variable in $[0, 1]$
$\overline{\alpha}$	waning immunity rate	variable in $[0, \infty)$
β	transmission rate	variable in $[0, \infty)$

Rescaling the model by measuring time in units of duration of infection, $t = T(\tau + \mu)$, we reduce the number of parameters and obtain a nondimensional system, where $e = \frac{\mu}{\tau+\mu}$ and $\alpha = \frac{\bar{\alpha}}{\tau+\mu}$ become nondimensional parameters. The model becomes

$$\begin{cases} \dfrac{dS}{dt} = e - R_0 IS - eS + \alpha R \\ \dfrac{dI}{dt} = R_0 IS + \sigma R_0 IR - I \\ \dfrac{dR}{dt} = (1 - e) I - (e + \alpha) R - \sigma R_0 IR. \end{cases}$$

We shall refer to this system as the rescaled SIRIS model. Note that the system becomes a standard SIR model at $\alpha = 0$ and $\sigma = 0$, and the SIS-type model corresponds to $\alpha \to \infty$ or $\sigma = 1$, when

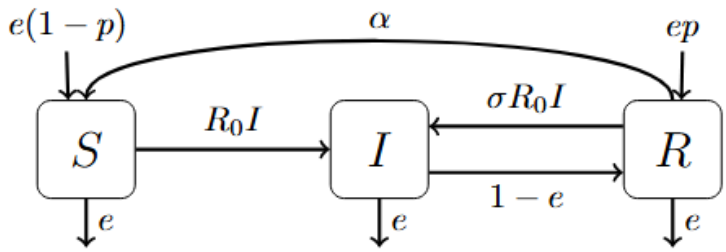

Figure 1. Schematic representation of the SIRISp Model 2.5.

aggregating S and R as the susceptible class. The temporary immunity model is retrieved at $\sigma = 0$ (and $\alpha \neq 0$), and the partial immunity model is obtained at $\alpha = 0$ (and $\sigma \neq 0$). A slightly different version of this model was proposed in [27], where temporary immunity is implemented so that the SIS limit appears more naturally.

We assume that the vaccine confers the same protection as the natural infection; hence, at each point in time, a proportion $p(t)$ of the newborns is vaccinated and enters the recovered class, whereas the remainder will become susceptible. Finally, since the total population is constant, we can reduce the model to the first two equations. Therefore, by introducing vaccination in the SIRIS model, the system can be written as

$$\begin{cases} \dfrac{dS}{dt} = e(1 - p(t)) - R_0 IS - eS + \alpha(1 - S - I) \\ \dfrac{dI}{dt} = R_0 IS + \sigma R_0 I(1 - S - I) - I. \end{cases} \tag{2.2}$$

See Figure 1 for a schematic representation of the model.

Individuals' choices on whether or not to vaccinate their newborns are modeled by an imitation dynamics approach, as in [15, 17, 26],

$$\frac{dp}{dT} = Kp(1 - p)\Delta E, \tag{2.3}$$

depending on the payoff function $\Delta E = E(V) - E(NV)$ that represents the difference in payoffs between the strategies of vaccinating (V) and not vaccinating (NV). Parameter K is the social-learning rate, which determines how quickly individuals will switch strategies if the strategy they're switching to offers a higher payoff than their current one. The payoffs are defined as the additive inverse of the perceived expected costs associated with vaccination and infection. Equation 2.3 can be derived from the replicator equation [15, 22, 28].

Alternatively, the decision-making process underlying strategy selection can be conceptualized as a transmissible trait. The population is stratified into two subgroups, p and q, corresponding to individuals choosing strategies V and NV, respectively. The transmission of opinions regarding strategy selection occurs at a rate proportional to both the payoff difference and the interaction frequency between the two subpopulations. The direction of transmission is determined by the strategy with the

higher payoff difference ΔE. The resulting ideas-transmission model is

$$\begin{cases} \dfrac{dp}{dT} = Kpq\Delta E, \\ \dfrac{dq}{dT} = -Kpq\Delta E. \end{cases}$$

Given that the total population is partitioned into two mutually exclusive groups ($q = 1 - p$), the model simplifies to Equation 2.3.

Following the reasoning in [26], we consider that the payoff associated with NV depends on the perceived cost of infection r_i for each individual, and the probability of being infected

$$E(NV) = -r_i\Pi_p^{nv}.$$

The payoff associated with V depends on the perceived cost of vaccination r_v for each individual, on r_i, and on the probabilities of being infected due to immunity loss or by reinfection, $\Pi_p^{v,\alpha}$ and $\Pi_p^{v,\sigma}$, respectively,

$$E(V) = -\left(r_v + r_i(\Pi_p^{v,\alpha} + \Pi_p^{v,\sigma})\right).$$

Table 2 shows a description of the imitation dynamic parameters.

Table 2. Imitation dynamics parameters.

Parameters	Description	Values
K	social-learning rate	variable in $(0, \infty)$
r_i	individual perceived cost of infection	1
r_v	individual perceived cost of vaccination	variable in $(0, 1)$

The infection probabilities are constructed from the System 2.2 depending on the exit times of the S and R states, assuming a change of state. For clarity, follow the schematic representation of the model in Figure 1. The probability of infection for non-vaccinated individuals is the proportion of individuals in compartment S that are infected, R_0IS, over all individuals who leave that compartment

$$\Pi_p^{nv} = \frac{R_0IS}{R_0IS + eS} = \frac{R_0I}{R_0I + e}.$$

The probability of infection due to loss of immunity for vaccinated individuals is the proportion of individuals that leave compartment R to S due to loss of immunity, αR, over all individuals who leave that compartment, multiplied by the probability of infection while in S

$$\Pi_p^{v,\alpha} = \frac{\alpha R}{\sigma R_0IR + (e + \alpha)R}\frac{R_0IS}{R_0IS + eS} = \frac{\alpha}{\sigma R_0I + e + \alpha}\frac{R_0I}{R_0I + e}.$$

Finally, the probability of infection due to partial immunity for vaccinated individuals is the proportion of individuals that leave compartment R to I due to reinfection, σR_0IR, divided by all individuals who leave that compartment

$$\Pi_p^{v,\sigma} = \frac{\sigma R_0IR}{\sigma R_0IR + (e + \alpha)R} = \frac{\sigma R_0I}{\sigma R_0I + e + \alpha}.$$

Temporary and partial immunity can theoretically lead to infinite cycles of repeated infections. For simplicity, and since it will be common to all routes of infection, we consider that both vaccinated and non-vaccinated individuals only take into account the probability of the first infection.

Thus, the payoff difference ΔE can be expressed as

$$\begin{aligned}\Delta E &= -r_v - r_i(\Pi_p^{v,\alpha} + \Pi_p^{v,\sigma}) - (-r_i\Pi_p^{nv}) \\ &= r_i\left(\Pi_p^{nv} - (\Pi_p^{v,\alpha} + \Pi_p^{v,\sigma}) - \frac{r_v}{r_i}\right) = r_i(\pi_p - r),\end{aligned}$$

where r is the relative perceived cost of vaccination compared to infection for each individual. In the particular case of $\sigma = \alpha = 0$, we get the same payoff function as in [26].

Equation 2.3 can thus be rewritten as

$$\frac{dp}{dt} = kp(1-p)[\pi_p - r], \tag{2.4}$$

where $k = \dfrac{Kr_i}{\tau + \mu}$ is the re-scaled social-learning rate and π_p is given by

$$\pi_p = \pi_p(I) = \frac{R_0 I}{R_0 I + e} - \left(\frac{\alpha}{\sigma R_0 I + e + \alpha}\frac{R_0 I}{R_0 I + e} + \frac{\sigma R_0 I}{\sigma R_0 I + e + \alpha}\right) = \frac{e(1-\sigma)R_0 I}{(R_0 I + e)(\sigma R_0 I + e + \alpha)}.$$

We assume that the perceived cost of vaccination is positive and always less than the perceived cost of infection $0 < r_v < r_i$, hence, $r \in (0, 1)$.

Finally, from Equations 2.2 and 2.4, we obtain

$$\begin{cases} \dfrac{dS}{dt} = e(1-p) - R_0 IS - eS + \alpha(1 - S - I) \\ \dfrac{dI}{dt} = R_0 IS + \sigma R_0 I(1 - S - I) - I \\ \dfrac{dp}{dt} = kp(1-p)[\pi_p - r], \end{cases} \tag{2.5}$$

that we refer to as the **SIRISp model**, which is a generalization of the SIRp model studied in [26].

When vaccination in the SIRIS model is assumed to be constant (equivalent to take k=0), one of two scenarios might occur: either immunity is solely granted by infection ($p(0) = 0$), or it is conferred by constant immunization coverage ($p(0) > 0$). In the former scenario, there are two equilibria: a stable disease-free equilibrium when $R_0 < 1$ and a stable endemic equilibrium when $R_0 > 1$ [27]. In the latter scenario, the system admits both a disease-free equilibrium with vaccination and an endemic equilibrium with vaccination, whose stability depends on whether R_0 lies below or above a vaccination-dependent critical threshold. If R_0 is below this threshold, the disease-free equilibrium is stable and the infection eventually dies out, leading to elimination. Conversely, if R_0 exceeds the threshold, the endemic equilibrium is stable and the disease persists in the population. A complete analysis of the SIRIS model, in a slightly different formulation from the one considered here, can be found in [27].

In our model, parameters e, α, and k are the rates in units of the average infectious period $1/(\tau+\mu)$, of population renewal, waning of immunity, and social learning, respectively. For example, $\alpha = 1/2$ means that on average it takes two infectious periods to lose immunity. See Table 3 for further details.

Table 3. Parameters of the rescaled SIRISp Model 2.5, considering $t = T(\tau+\mu)$, where $1/(\tau+\mu)$ is the average infectious period.

Parameters	Description
$e = \frac{\mu}{\tau+\mu} = 0.0278$	birth/mortality rate
$\alpha = \frac{\overline{\alpha}}{\tau+\mu}$	waning immunity rate
σ	partial immunity reduction factor
$R_0 = \frac{\beta}{\tau+\mu}$	basic reproduction number
$k = \frac{r_i K}{\tau+\mu}$	social-learning rate
$r = r_v/r_i$	individual relative perceived cost

In the next sections, we start by studying the equilibria stability of the SIRISp model. We then examine how the system's dynamic changes depending on the social learning and the relative perceived cost for different scenarios of partial and/or temporary immunity. Finally, we assess the effects of temporary immunity more thoroughly, emphasizing the conditions that allow for instability and oscillatory behavior.

3. Equilibria and stability of the model

The model has two disease free equilibria and three endemic equilibria. To study the stability of the equilibria we use the Jacobian matrix of System 2.5

$$J(S,I,p) = \begin{bmatrix} -IR_0 - \alpha - e & -R_0S - \alpha & -e \\ -IR_0\sigma + IR_0 & -IR_0\sigma + R_0S + R_0\sigma(-I - S + 1) - 1 & 0 \\ 0 & -kp(1-p)\pi_p(I,p)\frac{I^2R_0^2\sigma - e(\alpha+e)}{I(IR_0+e)(IR_0\sigma+\alpha+e)} & k(1-2p)\Big(\pi_p(I,p) - r\Big) \end{bmatrix}.$$

Disease-free equilibria

1. Disease-free with no vaccination at equilibrium

$$E^{\mathrm{df}_0} := (1,0,0).$$

The eigenvalues of $J(E^{\mathrm{df}_0})$ are: $-(\alpha+e)$, $-kr$, and $R_0 - 1$. So, the disease-free equilibrium E^{df_0} is stable for $R_0 < 1$ and unstable for $R_0 > 1$.

2. Disease-free with complete vaccination at equilibrium

$$E^{\mathrm{df}_1} := \left(\frac{\alpha}{e+\alpha}, 0, 1\right).$$

This equilibrium is always unstable since $rk > 0$ is an eigenvalue of the Jacobian matrix $J(E^{\mathrm{df}_1})$.

Endemic equilibria

From the first two equations in System 2.5, the endemic equilibria (S^*, I^*, p^*) will verify

$$S^* = \frac{e\,(1-p^*) + \alpha\,(1-I^*)}{R_0 I^* + e + \alpha} \left(= \frac{1 - \sigma R_0\,(1-I^*)}{R_0(1-\sigma)},\ \text{if } \sigma \neq 1 \right). \tag{3.1}$$

For $\sigma \neq 1$, these two expressions give the same value, hence, I^* must be a root of the polynomial

$$\mathcal{P}^*(I) = \mathcal{P}^{p^*}(I) = a_2 I^2 + a_1 I + a_0 \tag{3.2}$$

with

$$\begin{aligned} a_2 &= \sigma R_0^2 (\geq 0), \\ a_1 &= R_0(1 - \sigma R_0 + e\sigma + \alpha), \\ a_0 &= (1-R_0)(e+\alpha) + p^* R_0 e(1-\sigma). \end{aligned}$$

An endemic equilibrium (S^*, I^*, p^*) is feasible when $S^*, I^* \geq 0$, $S^* + I^* \leq 1$, and $p^* \in [0,1]$. Using the expression for S^* given by Equation 3.1, we get that $S^* + I^* \leq 1$ is equivalent to $I^* \leq 1 - \frac{1}{R_0}$ and that $S^* \geq 0$ is equivalent to $I^* \geq 1 - \frac{1}{\sigma R_0}$. Since we must have $I^* > 0$, we conclude that (S^*, I^*, p^*) is feasible if, and only if, $I^* \in \left(\max\left\{0, 1 - \frac{1}{\sigma R_0}\right\}, 1 - \frac{1}{R_0}\right]$. This interval for I^* gives values in $(0,1)$ for every $R_0 > 1$.

Considering $\sigma = 1$, where we recover the SIS model, the values of p and α are not relevant, since from the point of view of infection, it is indifferent to be susceptible or recovered. Then,

$$\begin{aligned} \mathcal{P}^*(-\infty) = \mathcal{P}^*(+\infty) &= +\infty, \\ \mathcal{P}^*(0) &= (\alpha+e)(1-R_0) < 0 \text{ and} \\ \mathcal{P}^*\left(1 - \frac{1}{R_0}\right) &= 0. \end{aligned}$$

We conclude that $I^* = 1 - \frac{1}{R_0}$ is the only feasible endemic equilibrium (the SIS endemic equilibrium).

Considering $\sigma = 0$, $\mathcal{P}^*$ is a first degree polynomial and

$$I^* = \frac{(\alpha+e)(R_0-1) - p^* e R_0}{R_0(1+\alpha)},$$

which is feasible if $p^* < \frac{1}{e}(\alpha+e)\left(1 - \frac{1}{R_0}\right)$.

Considering $\sigma \in (0,1)$, then

$$\begin{aligned} \mathcal{P}^*(-\infty) = \mathcal{P}^*(+\infty) &= +\infty, \\ \mathcal{P}^*\left(1 - \frac{1}{\sigma R_0}\right) &= -(1-\sigma)\left(R_0 e(1-p^*) + \frac{\alpha}{\sigma}\right) < 0, \\ \mathcal{P}^*\left(1 - \frac{1}{R_0}\right) &= (1-\sigma)\left(R_0 e p^* + (R_0-1)(1-e)\right) > 0 \text{ and} \\ \mathcal{P}^*(0) &= (\alpha+e)(1-R_0) + R_0 e p^*(1-\sigma). \end{aligned}$$

We conclude that if $R_0\sigma > 1$, there is exactly one feasible I^* for each p^*. If $R_0\sigma \leq 1$, there is at most one feasible I^* for each p^* if $\mathcal{P}^*(0) < 0$, and none otherwise.

The following endemic equilibria can be computed by taking the zeros of the right member of the last equation in System 2.5.

1. Endemic equilibrium with no vaccination

$$E^{\text{en}_0} := (S^{\text{en}_0}, I^{\text{en}_0}, p^{\text{en}_0})$$

given by

$$\begin{aligned} S^{\text{en}_0} &= \frac{e + \alpha(1 - I^{\text{en}_0})}{e + \alpha + R_0 I^{\text{en}_0}} \\ p^{\text{en}_0} &= 0, \end{aligned}$$

where I^{en_0} is the only feasible zero of $\mathcal{P}^{\text{en}_0}(I) = \mathcal{P}^0(I)$.
The eigenvalues of the Jacobian matrix at E^{en_0} are the roots of

$$char_J(\lambda, E^{\text{en}_0}) = char_{\Delta_{33}}(\lambda, E^{\text{en}_0})\,(J_{33}\,(E^{\text{en}_0}) - \lambda)\,,$$

with

$$char_{\Delta_{33}}(\lambda, S, I, p) = \lambda^2 + \lambda\,(IR_0(\sigma + 1) + \alpha + e) + I^2R_0^2\sigma + IR_0\sigma(\alpha + e) + IR_0(1-\sigma)\,(R_0S + \alpha) \quad (3.3)$$

since the last row has only one nonzero entry at

$$J_{33}(E^{\text{en}_0}) = k\left(\pi_p(I^{\text{en}_0}, 0) - r\right).$$

Observe that the coefficients of $char_{\Delta_{33}}$ are positive and, by the Ruth-Hurwitz stability criterion, have roots with negative real part.
Hence, the equilibrium is stable if

$$\pi_p(I^{\text{en}_0}, 0) < r. \quad (3.4)$$

2. Endemic equilibrium with full vaccination

$$E^{\text{en}_1} := (S^{\text{en}_1}, I^{\text{en}_1}, p^{\text{en}_1})$$

given by

$$\begin{aligned} S^{\text{en}_1} &= \frac{\alpha(1 - I^{\text{en}_1})}{e + \alpha + R_0 I^{\text{en}_1}} \\ p^{\text{en}_1} &= 1, \end{aligned}$$

where I^{en_1} is the only feasible zero of $\mathcal{P}^{\text{en}_1}(I) = \mathcal{P}^1(I)$. This feasible equilibrium exists and is unique if, and only if, $R_0 > 1 + \frac{e(1-\sigma)}{\sigma e + \alpha} (> 1)$.
The eigenvalues of the Jacobian matrix at E^{en_1} can be analyzed in the same way as in the previous equilibrium, concluding that E^{en_1} is stable if

$$\pi_p(I^{\text{en}_1}, 1) > r. \quad (3.5)$$

3. Endemic equilibrium with intermediate vaccination

$$E^{\mathrm{en}_p} := (S^{\mathrm{en}_p}, I^{\mathrm{en}_p}, p^{\mathrm{en}_p})$$

given by

$$S^{\mathrm{en}_p} = \frac{1-\sigma R_0\,(1-I^{\mathrm{en}_p})}{R_0(1-\sigma)} = \frac{e(1-p^{\mathrm{en}_p})+\alpha(1-I^{\mathrm{en}_p})}{e+\alpha+R_0 I^{\mathrm{en}_p}}.$$

This equilibrium verifies $\pi_p(I^{\mathrm{en}_p}, p^{\mathrm{en}_p}) = r$, corresponding to the interior Nash equilibrium from the associated static model. Hence, I^{en_p} has to verify the condition

$$(1-\sigma)R_0 I\left(R_0 I + e + \frac{e}{r}\right) = (R_0 I + e + \alpha)\,(R_0 I + e) \tag{3.6}$$

while in the interval $(0, 1]$. Both members in Equation 3.6 can be represented as parabolas, with the concavity of the first one given by $(1-\sigma)R_0^2$. For some choice of parameters, those parabolas can intersect successively in one, two, one, and no values of $I^{\mathrm{en}_p} \in (0, 1]$, when varying σ from 0 to 1, giving rise to a fold-bifurcation.
More precisely, I^{en_p} is a positive zero of the polynomial

$$Q^{\mathrm{en}_p}(I) = b_2 I^2 + b_1 I + b_0$$

with

$$\begin{aligned} b_2 &= \sigma r R_0^2\ (\geq 0),\\ b_1 &= R_0[r(e+\alpha+e\sigma) - e(1-\sigma)],\\ b_0 &= er(e+\alpha)\ (>0)\ . \end{aligned}$$

The value of p^{en_p} can be computed from $\mathcal{P}^{p^{\mathrm{en}_p}}(I^{\mathrm{en}_p}) = 0$, with $\mathcal{P}$ defined in Expression 3.2.
For $\sigma = 0$, we have only a first-order polynomial, and we get

$$\begin{aligned} S^{en_p}_{\sigma=0} &= \frac{1}{R_0},\\ I^{en_p}_{\sigma=0} &= \frac{1}{R_0}\frac{re(\alpha+e)}{e-r(\alpha+e)} \text{ and}\\ p^{en_p}_{\sigma=0} &= \frac{1}{R_0}\frac{\alpha+e}{e}\frac{(R_0-1)(e-r(\alpha+e))-re(\alpha+1)}{e-r(\alpha+e)}, \end{aligned}$$

which is feasible if $r \in \left(\max\left\{0, \frac{e}{\alpha+e}\frac{\alpha(R_0-1)-e}{\alpha(R_0-1+e)}\right\}, \frac{e}{\alpha+e}\frac{R_0-1}{R_0-1+e}\right)$.

For $\sigma > 0$, we can have two distinct feasible equilibria $E^{\mathrm{en}_p\pm}$, with $I^{en_p\pm} = \frac{-b_1 \pm \sqrt{b_1^2-4b_2b_0}}{2b_2}$, one ($E^{en_p} = E^{en_p+}$), or none, depending on the parameters (one can establish conditions for both possibilities, analyzing when Q^{en_p} has feasible roots; in particular, by the Descartes' rule of signs, $b_1 < 0$ is a necessary condition for having at least one feasible equilibrium).
The eigenvalues of the Jacobian matrix at E^{en_p} are the roots of

$$char_J(\lambda, E^{\mathrm{en}_p}) = \lambda\, char_{\Delta_{33}}(\lambda, E^{\mathrm{en}_p}) + (1-\sigma)kp^{\mathrm{en}_p}(1-p^{\mathrm{en}_p})\frac{R_0 e I^{\mathrm{en}_p}(2b_2 I^{\mathrm{en}_p}+b_1)}{(I^{\mathrm{en}_p}R_0+e)(I^{\mathrm{en}_p}R_0\sigma+\alpha+e)}$$

$$= \lambda^3 + d_2\lambda^2 + d_1\lambda + d_0,$$

with $char_{\Delta_{33}}(\lambda, S, I, p)$ given by Expression 3.3. By the Routh-Hurwitz stability criterion, the equilibria is stable only if all the coefficients of $char_J$ are positive, so we must have $I^{en_p} > \frac{-b_1}{2b_2}$ and we conclude that, even if feasible, E^{en_p-} is always unstable. As for E^{en_p+}, when feasible, again by the Ruth-Hurwitz stability criterion, it will be stable if, and only if,

$$d_1\, d_2 - d_0 > 0. \tag{3.7}$$

Observe that this condition and, thus, the stability of E^{en_p+}, depends on k.

To summarize the stability results, we will use the following color code to mark the stability region of each equilibrium, when feasible:

E^{df_0} - disease-free equilibrium, when $R_0 < 1$.
E^{en_0} - endemic equilibrium with no vaccination, when $\pi_p(I^{en_0}, 0) < r$ (Equation 3.4);
E^{en_1} - endemic equilibrium with full vaccination, when $\pi_p(I^{en_1}, 1) > r$ (Equation 3.5);
E^{en_p} - endemic equilibrium with intermediate vaccination, when $d_1\, d_2 - d_0 > 0$ (Equation 3.7).

For $\sigma > 0$, these stability regions can overlap and we can have:

E^{en_0} and $E^{en_{p+}}$ - bistability between the endemic equilibria with no vaccination and with intermediate vaccination;
E^{en_0} and E^{en_1} - bistability between the endemic equilibria with no vaccination and with full vaccination;
E^{en_0} and periodic orbits - endemic equilibrium with no vaccination is stable and stable periodic orbits can coexist.

In the white regions, all equilibria are unstable and it can exist stable periodic orbits.

Throughout this work, for illustration of the results, we fix $e = 0.0278$, since $e = \mu/(\tau+\mu)$, $\mu = 1/35$ yrs^{-1} and $\tau = 1$ yrs^{-1}, according to Table 1. This corresponds to the parameter values used for the previous SIRp model in [26], which coincides with the case $\sigma = \alpha = 0$. While fixing μ, τ (and, consequently, e), and r_i, the remaining parameters R_0, α, σ, k, and r will be variable, over which the bifurcation analysis will be conducted. See Table 3 for further details.

In Figure 2, we show the bifurcation diagram on the (R_0, r)-plane, for different values of k, α, and σ. Higher values of the relative perceived cost r promote vaccination refusal. When immunity to infection is temporary, low relative perceived cost and high transmissibility promote full vaccination. For intermediate values of the relative perceived cost, the intermediate vaccination equilibrium can be stable, but it loses stability for higher values of R_0 or k (white region). Partial immunity enhances vaccination refusal. Moreover, the complexity of the model behavior increases as the stability region of the endemic equilibrium with no vaccination overlaps with the stability region of the endemic equilibrium with intermediate or full vaccination. In these cases, results will crucially depend on initial conditions.

In the instability region (in white), we can have periodic or chaotic behavior, as illustrated for different parameter combinations in Figure 3, for fixed $R_0 = 4$ and $k = 2.5$. This region is amplified by the social-learning rate k. This choice of parameters allows for the direct comparison with the chaotic orbit obtained in [26], for the particular case $\sigma = \alpha = 0$ (Figure 3(d)).

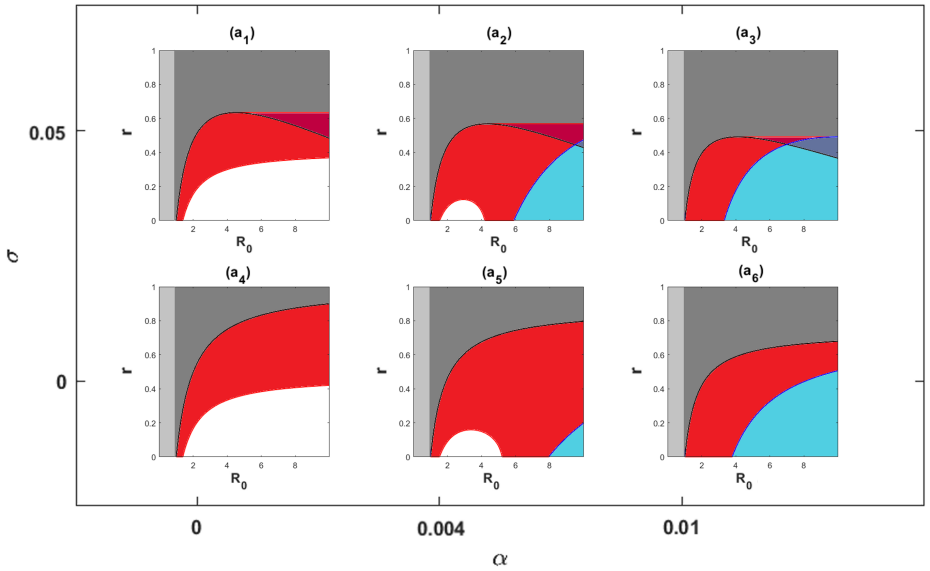

(a) $k = 0.1$

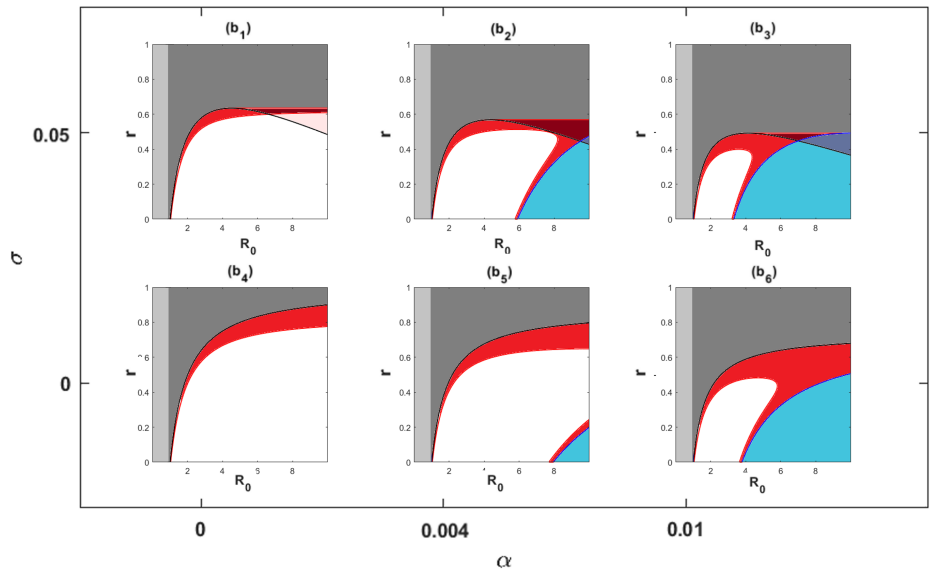

(b) $k = 1$

Figure 2. Bifurcation diagram on the (R_0, r)-plane with different combinations of α and σ, for: (a) $k = 0.1$ and (b) $k = 1$. Asymptotic stability region for: E^{df_0} - disease-free equilibrium; E^{en_0} - endemic equilibrium with no vaccination; E^{en_1} - endemic equilibrium with full vaccination; E^{en_p} - endemic equilibrium with intermediate vaccination. In the white regions, all equilibria are unstable. Intersection of stability regions: E^{en_0} and $E^{en_{p+}}$ - bistability between the endemic equilibria with intermediate and with no vaccination; E^{en_0} and E^{en_1} - bistability between the endemic equilibria with no vaccination and with full vaccination; E^{en_0} and periodic orbits - equilibrium E^{en_0} is stable and stable periodic orbits can coexist.

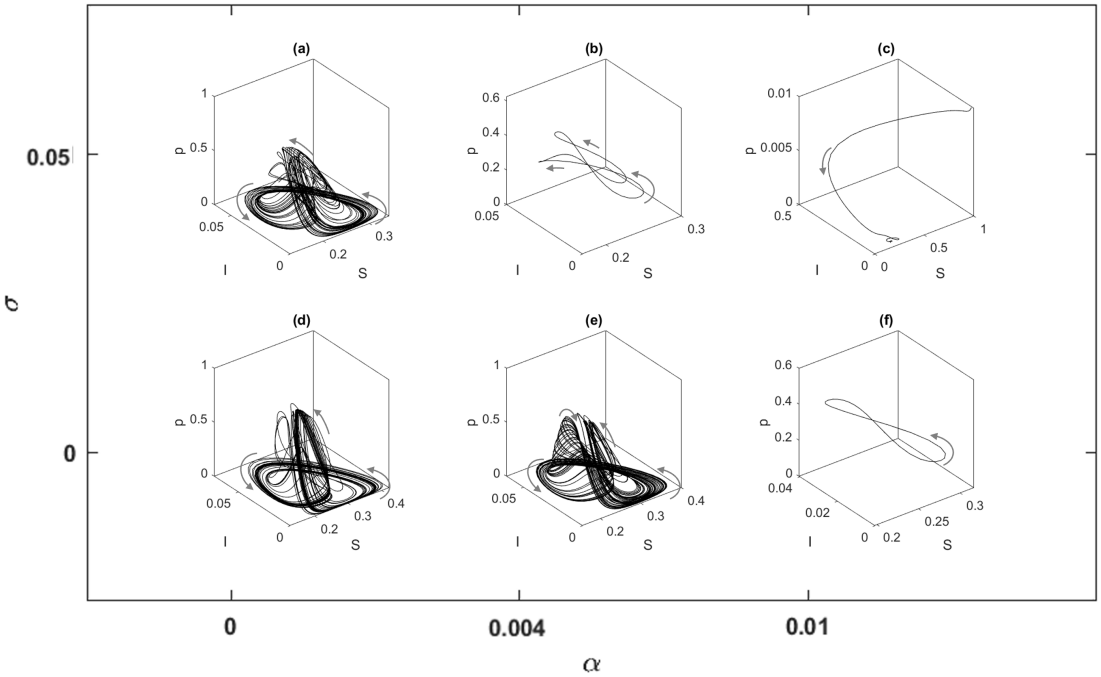

Figure 3. Time simulations in the (S, I, p) phase space, for different combinations of α and σ, with $r = 0.5$ and $k = 2.5$. Epidemiological parameters are $e = 0.0278$ ($e = \mu/(\tau + \mu)$, $\mu = 1/35$ yrs^{-1} and $\tau = 1$ yrs^{-1}), and $R_0 = 4$.

4. Impact of the social-learning

In this section, we analyze the impact of the social-learning rate in the stability of the endemic equilibria of the SIRISp model. For illustration purposes in the follow-up results, we fix $R_0 = 4$. Figure 4 shows the bifurcation diagram on the (k, r)-plane for different values of α and σ. We can observe that for a higher relative perceived cost r, individuals choose not to vaccinate. For intermediate values of the relative perceived cost, vaccination can become advantageous, and the intermediate vaccination equilibrium can be stable. However, by increasing the social-learning rate k, it loses its stability and crosses into the white region. This is the same phenomenon reported in [17, 26].

Temporary immunity leads to the stability of the full vaccination equilibrium at low relative perceived cost (indicated in blue). In this scenario, although all individuals choose to be vaccinated, the disease remains endemic due to temporary immunity. In Figure 4, we can observe that by increasing the rate of loss of immunity α (from (a) to (d) or from (e) to (h)), the instability region, marked in white, is shifted to higher values of k. Moreover, the stability regions of the endemic equilibria with non or complete vaccination increase until their limit coincides, enhanced by partial immunity.

Time simulations such as those in Figure 3 had already shown apparent chaotic behavior followed by stable periodic orbits as both α and σ increased. Figure 5 exhibited with further detail the underlying dynamics of the system for the cases of only partial immunity ($\alpha = 0$ and $\sigma = 0.01$), only temporary immunity ($\alpha = 0.001$ and $\sigma = 0$), and both partial and temporary immunity ($\alpha = 0.01$ and $\sigma = 0.01$).

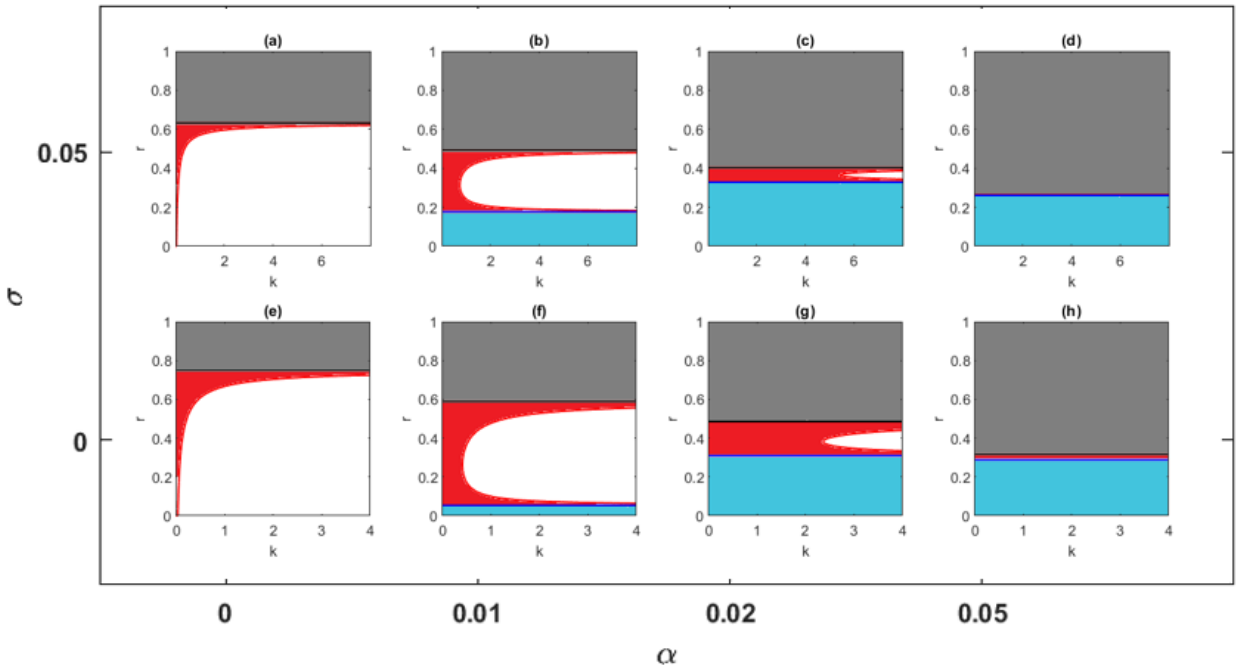

Figure 4. Bifurcation diagram on the (k, r)-plane for different combinations of α and σ. Asymptotic stability region for: E^{en_0} - endemic equilibrium with no vaccination; E^{en_1} - endemic equilibrium with full vaccination; E^{en_p} - endemic equilibrium with intermediate vaccination. In white regions, all equilibria are unstable. Epidemiological parameters are $e = 0.0278$ and $R_0 = 4$.

For each case, we plot the local minima and maxima of the infectious and vaccinated, while varying k. Moreover, we compute the Lyapunov exponents to better identify the chaotic regions.

Lyapunov exponents were introduced by Aleksandr Lyapunov in 1892, as a means to quantify the rate of divergence over time of nearby trajectories of a dynamical system. A positive Lyapunov exponent is a strong indicator of sensitivity to initial conditions, which is a common trait attributed to chaos. In the context of epidemiological modeling, these exponents have gained significant traction over the years, particularly in nonautonomous models with seasonal dynamics. For instance, Aguiar et al. [29] demonstrated the existence of chaotic regions in a dengue model using Lyapunov exponents. Duarte et al. [30] explored chaotic regimes and the predictability of attractor emergence, while Stollenwerk et al. [31] showed that seasonality can lead to chaos through periodic doubling bifurcations and the coexistence of multiple attractors in models with mutating pathogens. The developed code for the computation and calculation of the Lyapunov exponents in our work uses an open-source Github library package [32] inspired by Benettin et. al's algorithm [33].

Figures 5 (a_1) and 5 (a_2) show the bifurcation diagrams for p and I, when $\alpha = 0$ and $\sigma = 0.01$. As k increases, we observe the onset of period-doubling bifurcations, which become increasingly more frequent until irregular oscillations are present. We can confirm chaos onset as, at this point, one of the Lyapunov exponents becomes positive while still having one at zero in Figure 5 (a_3). We can also observe that whenever chaotic behavior seems to cease, the maximum Lyapunov exponent falls

back down to zero and all the other remain or become negative. When $\alpha = 0.001$ and $\sigma = 0$, the same behavior occurs, depicted in Figures 5 (b_i). However, as we bring α and σ to 0.01, shown in Figures 5 (c_1) and 5 (c_2), we can only observe simple periodic behavior and subsequently no positive Lyapunov exponents, in Figure 5 (c_3). This leads to the conclusion that, for this model, chaos is highly sensitive to small changes in the loss of immunity and reinfection parameters.

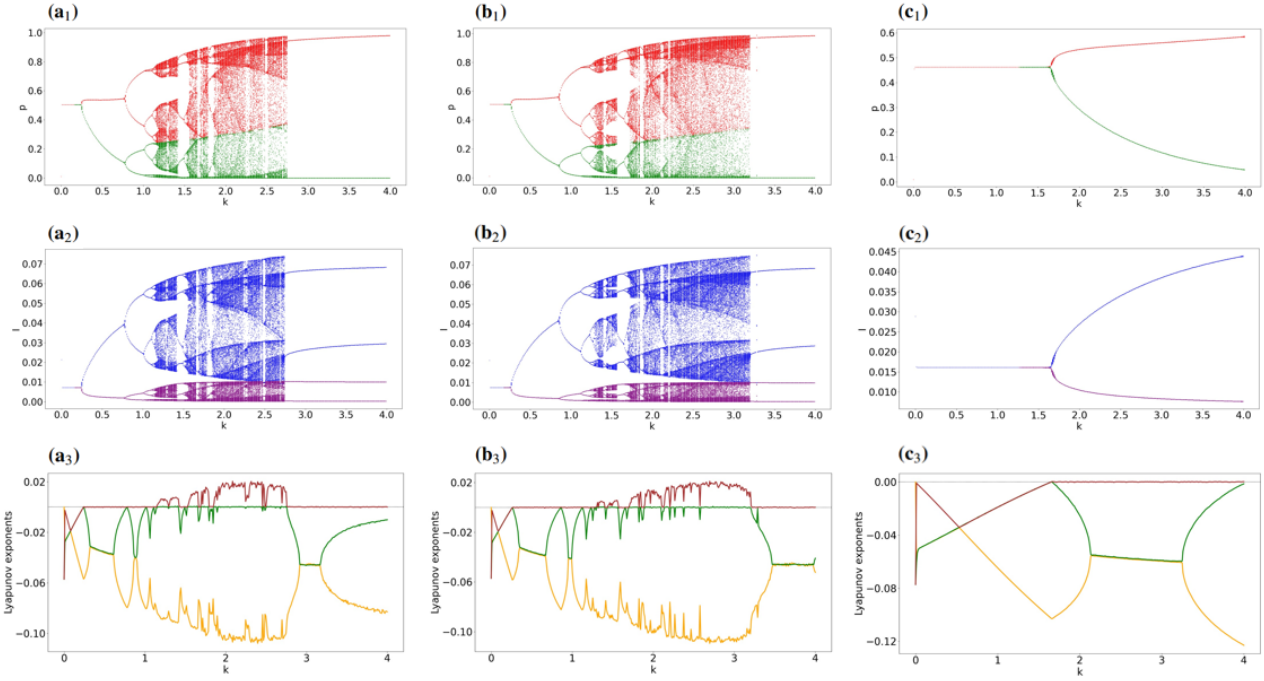

Figure 5. Bifurcation diagrams and Lyapunov exponents on parameter k with $r = 0.5$, for three different cases: (a_i). $\alpha = 0$, $\sigma = 0.01$; (b_i). $\alpha = 0.001$, $\sigma = 0$, and (c_i) $\alpha = 0.01$, $\sigma = 0.01$. In (a_1), (b_1), (c_1), the proportion of vaccinated individuals p (local maximum and minimum in red and green, respectively). In (a_2), (b_2), (c_2), the proportion of infected individuals I (local maximum and minimum in blue and purple, respectively). In (a_3), (b_3), (c_3), the Lyapunov exponents. Epidemiological parameters are $e = 0.0278$ and $R_0 = 4$.

As such, we can further analyze the Lyapunov exponents when varying α and σ in the (α, σ)-plane, to study to what extent the chaotic behavior can be sensitive to partial and temporary immunity. Figure 6 portrays the maximum Lyapunov exponent mapped over the (α, σ)-plane. The yellow parts of the map correspond to parameter combinations where positive Lyapunov exponents were detected, whereas the orange parts correspond to a zero maximum Lyapunov exponent, characteristic of regular periodic behavior. The parameter α seems to impose the strongest constraint when it comes to the emergence of chaos, since very few positive exponents were registered beyond $\alpha = 0.005$. Even though both parameters are interconnected, σ shows a little more leeway to the emergence of chaos, with positive exponents being registered as far as $\sigma = 0.05$ and beyond.

Moreover, from an epidemiological standpoint, the parameters σ and α have different interpretations and impacts. The parameter α is a rate, meaning small values correspond to very long durations of immunity, which may represent unrealistic scenarios when compared to the average human lifespan. In contrast, for σ, any value between 0 and 1 affects the system solely on how immunity is shaped by

the primary infection. It may even be reasonable to consider $\sigma > 1$ (a case not addressed in this study).

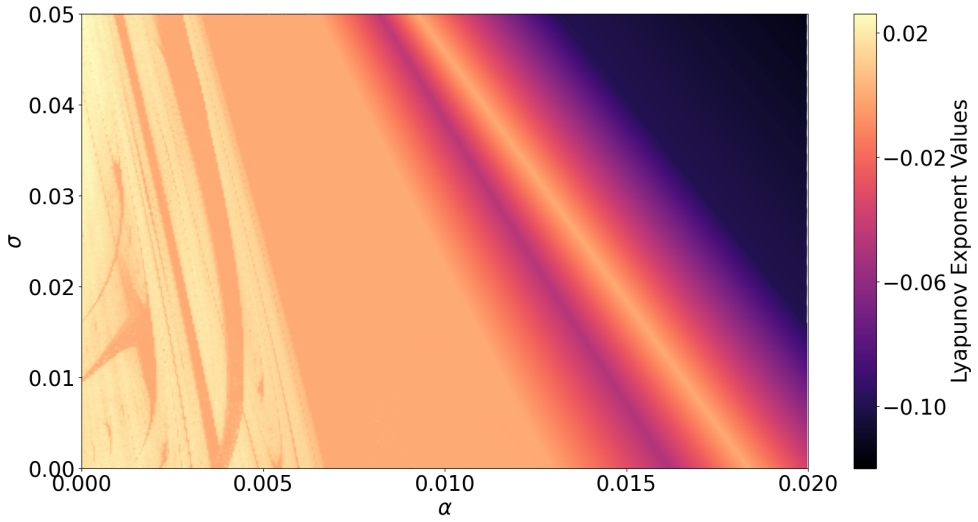

Figure 6. Maximum Lyapunov exponent on the (α, σ)-plane for $k = 2.5$. Epidemiological parameters are $e = 0.0278$ and $R_0 = 4$.

In a broader scope, in Figure 7, we represent the bifurcation diagram in the (α, σ)-plane, fixing $r = 0.5$ and $k = 2.5$. It confirms that the region of possible periodic and chaotic solutions seems restricted to high protection to reinfection and long immunity periods. We can also observe that the stability regions of the endemic equilibria E^{en_0} and E^{en_p} can overlap. There is a bistability region for the endemic equilibria with no or intermediate vaccination (E^{en_0} and $E^{\mathrm{en}_{p^+}}$) and a possible coexistence region of the stable equilibrium with no vaccination E^{en_0} and stable periodic orbits (E^{en_0} and stable periodic orbits). In a more general way, when considering partial immunity, the stability of the equilibria becomes more intricate, as described in Section 3. The bistability phenomena had already been reported in Reluga et al. [34] for a model with partial immunity conferred by vaccination and an equilibrium vaccination game.

Although chaos can still be registered for small values of loss of immunity and reinfection, these parameters seem to dampen chaos in the system and not the other way around. The $\alpha = 0$, $\sigma = 0$ case, previously studied in [26], had a prominent display of chaos, which leads us to believe the chaos registered in this work is but a remnant of a system falling back to an orderly periodic cycle, as these parameters become more relevant.

5. The role of temporary immunity

In the previous section, we observed that the region favorable to chaotic behavior appears to be restricted to low values of σ and α. In particular, we note that for the chosen parameters, the values of α are of the same order of magnitude as the rescaled death rate $e = 0.0278$. This would mean that the immunity conferred by the disease is almost lifelong, which has practical implications for the

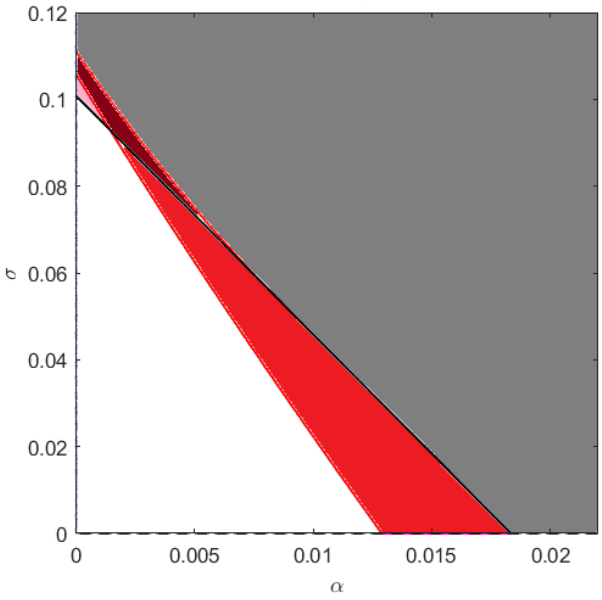

Figure 7. Bifurcation diagram on the (α, σ)-plane, with $r = 0.5$ and $k = 2.5$. Bistability region for: E^{en_0} and $E^{en_{p+}}$, the endemic equilibria with no or intermediate vaccination. Possible coexistence region of the stable equilibrium with no vaccination E^{en_0} and stable periodic orbits . Epidemiological parameters are $e = 0.0278$ and $R_0 = 4$.

applicability of these results. In this subsection, we will consider only temporary immunity ($\sigma = 0$) and explore, in more depth, the implications of varying α on the emergence of periodic and chaotic orbits.

In fact, for $\sigma = 0$, the stability conditions for the endemic equilibria can be further simplified. From Equations 3.4 and 3.5, we can obtain the analytic expression of the curves that mark the change in stability of the endemic equilibria E^{en_0} and E^{en_1}, for which the equalities hold

$$r_c^{\mathrm{en}_0} = \frac{e(R_0-1)}{(R_0-1)(e+\alpha)+e(\alpha+1)} \left(< \frac{e}{e+\alpha}\right)$$
$$r_c^{\mathrm{en}_1} = \frac{e(\alpha(R_0-1)-e)}{\alpha(R_0-1+e)(e+\alpha)}.$$

Note that these conditions are independent of k. Both expressions of the right side members are zero for the infimum value of R_0, for which the respective equilibrium is feasible, and are increasing with R_0, and both approach asymptotically the same supremum $\frac{e}{e+\alpha}$ as $R_0 \to +\infty$. Also, it is straightforward to check that

$$r_c^{\mathrm{en}_0} - r_c^{\mathrm{en}_1} = \frac{e^2}{\alpha\left((R_0-1)(\alpha+e)+e(\alpha+1)\right)} > 0, \qquad \text{for every } R_0 > \frac{\alpha+e}{e}.$$

In particular, $r_c^{\mathrm{en}_0} - r_c^{\mathrm{en}_1}$ decreases to 0 as $R_0 \to +\infty$. As previously shown, the (unique) endemic equilibrium with intermediate vaccination, E^{en_p}, is locally asymptotically stable if, and only if, $d_1\, d_2 -$

$d_0 > 0$; see Condition 3.7. When $\sigma = 0$, we can get the explicit expressions

$$\begin{aligned} d_2 =& \frac{(\alpha + e)(e - \alpha r)}{e - r(e + \alpha)}, \\ d_1 =& \frac{er(\alpha + e)(\alpha + 1)}{e - r(e + \alpha)}, \\ d_0 =& k\frac{\alpha r(\alpha + e)^2(R_0 - 1 + e)(\alpha(R_0 - 1) + e(R_0 + \alpha))}{R_0 e^2(e - r(e + \alpha))}(r_c^{\text{en}_0} - r)(r - r_c^{\text{en}_1}). \end{aligned}$$

Following the same argument as in [26], we conclude that, for $R_0 > 1$ and $\max\{0, r_c^{\text{en}_1}\} < r < r_c^{\text{en}_0}$, we have a supercritical Hopf bifurcation at

$$k = k_c := \frac{R_0 e^3(e - \alpha r)(\alpha + 1)}{\alpha(r - r_c^{\text{en}_1})(r_c^{\text{en}_0} - r)(R_0 - 1 + e)(e - r(e + \alpha))(\alpha(R_0 - 1) + e(R_0 + \alpha))}, \tag{5.1}$$

where the equilibrium E^{en_p} loses its stability and stable periodic orbits emerge. In Figure 4(e)-(g), we observe the Hopf bifurcation curve in the (k, r)-plane that limits the red region, for $\sigma = 0$.

Figure 8 shows the bifurcation diagram of equilibria and limit cycles in the (k, r)-plane, with $\alpha = 0.01$, detailing Figure 4(f). The boundary bifurcation curve BP_0 (black) marks the change in stability of E^{en_0} to E^{en_p}, as r decreases. The boundary bifurcation curve BP_1 marks the change in stability of E^{en_1} to E^{en_p}, as r increases. The Hopf bifurcation curve H corresponds to where E^{en_p} changes from stable to unstable, from left to right, with the emergence of stable periodic limit cycles. These limit cycles will have their period doubled at the flip F bifurcation curve, also called periodic doubling bifurcation. This curve marks the threshold at which a cascade of period doubling may occur and periodic behavior can further evolve into chaotic dynamics (see also Figure 5 for similar behavior). The results in Figure 8 were obtained by numerical continuation methods [35], using MatCont [36] and AUTO [37], and coincide with those we deduce analytically, in particular, Equation 5.1. The flip bifurcation curve F was obtained exclusively by numerical continuation.

Figure 9 shows the bifurcation diagram on the (r, α)-plane, for different values of the imitation rate k with $\sigma = 0$. Only for very high values of k, there is a narrow region where we have instability for higher values of α, and therefore the possibility of chaotic behavior.

Figure 10 shows the bifurcation diagram on the (k, α)-plane, for different values of the relative perceived cost $r \in \{0.2, 0.3, 0.5\}$, considering $\sigma = 0$. In Figure 10 (b), with relative perceived cost fixed to $r = 0.3$, we can see a second window of opportunity for stable limit cycles and chaotic orbits, within the instability region, for a higher social-learning rate and a shorter period of temporary immunity, e.g., $k = 40$ (≈ 41 times the infectious period) and $\alpha = 0.05$ (≈ 0.56 times the average life expectancy).

6. Discussion & future work

This study focused on the SIRISp model assuming temporary and/or partial immunity that incorporates behavioral responses to infection and vaccination perceived costs. As for the analogous SIR model [17,26], the system is able to accommodate periodic limit cycles and complex dynamics, including irregular and potentially chaotic oscillations, which emerge solely from the population's individual decisions regarding vaccination. However, this periodic and/or chaotic behavior mostly arises for low

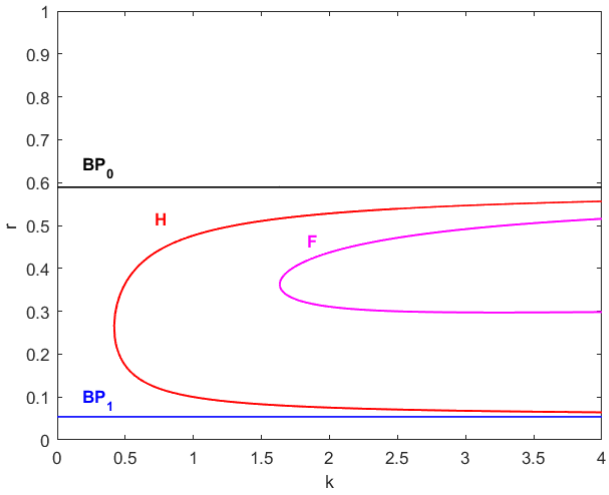

Figure 8. Bifurcation diagram in the (k, r)-plane for equilibria and limit cycles, with $\alpha = 0.01$, $\sigma = 0$. BP_0 - boundary bifurcation curve (in black); BP_1 - boundary bifurcation curve; H - Hopf bifurcation curve; F - flip bifurcation curve. Epidemiological parameters are: $R_0 = 4$, $e = 0.0278$.

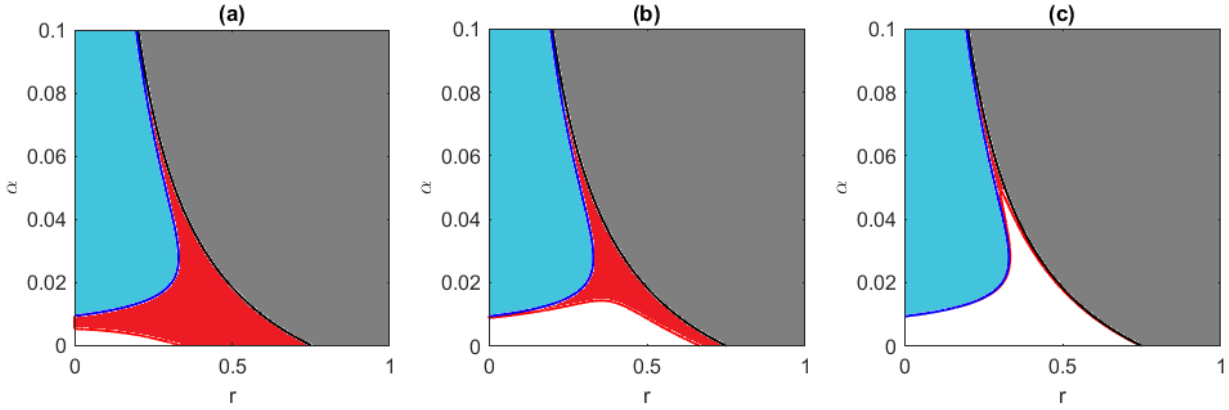

Figure 9. Bifurcation diagram on the (r, α)-plane with $\sigma = 0$ and for: (a) $k = 0.1$ (b) $k = 2.5$ and (c) $k = 30$. Stability regions of the endemic equilibria are marked by the color code. Epidemiological parameters are $e = 0.0278$ and $R_0 = 4$.

values of the parameters governing partial immunity (σ) and temporary immunity (α), with the latter corresponding to scenarios where immunity is almost permanent.

When immunity is temporary, that is, when $\alpha > 0$, the model admits an additional endemic equilibrium characterized by full vaccination coverage. This is the dominant equilibrium state for higher values of the basic reproduction number (R_0) and lower values of the relative perceived cost parameter r. An increase in α eliminates the intermediate vaccination equilibrium, suppressing chaotic dynamics and resulting in a globally stable endemic state with full vaccination. This suggests that temporary immunity plays a fundamentally stabilizing role in the system's dynamics.

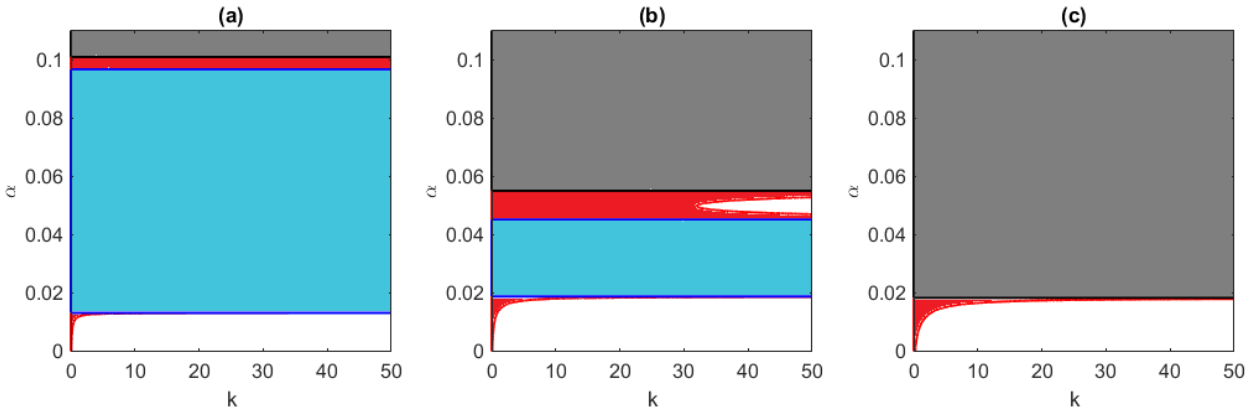

Figure 10. Bifurcation diagram on the (k, α)-plane, with $\sigma = 0$ and for: (a) $r = 0.2$, (b) $r = 0.3$, and (c) $r = 0.5$. Stability regions of the endemic equilibria are marked by the color code. Epidemiological parameters are $e = 0.0278$ and $R_0 = 4$.

Such stabilizing effects are consistent with results obtained in previous works on dengue transmission models. In particular, Aguiar et al. [38] showed that, within the regime of cross-protection ($\sigma < 1$), incorporating a short period of temporary cross-immunity leads to more regular epidemic behavior, whereas longer durations of cross-immunity can give rise to chaotic dynamics. Conversely to our work, the emergence of periodic and chaotic dynamics is driven by the interplay between strain competition and antibody-dependent enhancement, instead of deriving from human behavior.

The social-learning rate may significantly influence long-term disease outcomes, from steady or cyclic vaccine adherence to more erratic behavior, always below the elimination threshold. For infections where immunity wanes more rapidly and there is partial immunity, the model shows less erratic dynamics, restricted to low transmissibility (R_0) and higher social-learning rates. This scenario can be relevant to COVID-19 or seasonal influenza. However, for such diseases, sustained control requires repeated vaccination efforts extending to adult populations.

Within this study, the epidemiological parameters were selected to ensure comparability with the authors' previous work. More importantly, this choice reduces computation time and prevents integration instabilities, since the Lyapunov exponents were computed over large regions of the parameter space. Illustrations of the described dynamics can also be obtained using more realistic parameter values.

Overall, this study highlights the intricate interplay between social-learning rates and perceived costs, offering valuable perspectives on the dynamics of vaccination strategies. Our bifurcation analysis illustrates why social learning and perceived costs should be controlled (e.g., through vaccination and information campaigns, paid vaccines, media coverage), so that the population achieves a desirable public health state.

We emphasize that this model is intended as a baseline framework (or "null" scenario). With this perspective, the present study is not designed to represent any particular infectious disease. Instead, our goal is to provide a conceptual exploration of two mechanisms of immunity loss, namely, partial and temporary of immunity, which may arise in different epidemiological contexts. By analyzing these mechanisms in a general modeling setting, we aim to contribute to a qualitative understanding of the

potential effects that may be expected when the model is later tailored to specific infectious diseases.

These insights can be relevant for diseases such as measles or mumps. In several countries, the vaccine coverage for these diseases is close to the critical elimination threshold, and the vast majority of individuals in the recovered compartment acquire immunity through vaccination rather than natural infection. Although vaccine-induced immunity for these infections is typically long-lasting, it is not necessarily lifelong, and empirical evidence supports the occurrence of loss of immunity in highly vaccinated populations as seen in the works of Yang et al. [39], Mossong et al. [40], and Mossong and Muller [41]. Our model provides a unified representation of loss of immunity by allowing it to emerge from either reduced susceptibility (partial immunity) or finite duration of immunity (temporary immunity), without committing to a specific immunological mechanism. The findings provide a useful starting point for further investigation into how different parameters influence epidemic dynamics, with the potential to support more effective public health interventions and policy decisions.

It is also noteworthy that the present model assumes homogeneous infection and recovery metrics across the entire population. For most diseases, this assumption may be unrealistic, as different age groups or subpopulations can experience infection and recovery in distinct ways, as discussed in Chalub's work [14]. As previously affirmed, the current framework should be regarded as a baseline model to which more refined formulations, accounting for different heterogeneities, can be compared.

Future research should focus on disease-specific model construction and calibration to better assess the real-world relevance of the dynamic regimes identified here. In particular, the formulation of the payoff difference ΔE, which drives the vaccination dynamics, plays a crucial role in shaping the results. Since several alternative specifications have been proposed in the literature, a systematic comparison of these formulations and their consistency with empirical data would be highly valuable. Incorporating age-structured and periodic vaccination strategies into the model remains an important direction to pursue. Additionally, distinguishing between partial immunity and vaccine failure, as in Reluga's vaccination model [34], would provide a more realistic representation and further enrich future research in this area.

Use of AI tools declaration

The authors declare they have not used Artificial Intelligence (AI) tools in the creation of this article.

Acknowledgements

This work is funded by national funds through the FCT – Fundação para a Ciência e a Tecnologia, I.P., under the scope of the projects UID/00297/2025 (https://doi.org/.org/10.54499/UID/00297/2025) and UID/PRR/00297/2025 (https://doi.org/.org/10.54499/UID/PRR/00297/2025) (Center for Mathematics and Applications) and by the project "Mathematical Modelling of Multi-scale Control Systems: applications to human diseases (CoSysM3)", 2022.03091.PTDC (https://doi.org/.org/10.54499/2022.03091.PTDC), financially supported by national funds (OE), through FCT/MCTES. R Castelhano was supported by a Research Grant, ref. #NOVAID-B285, in the scope of the CoSysM3 Project.

Conflict of interest

The authors declare there is no conflict of interest.

References

1. *World Health Organization*, WHO COVID-19 dashboard – deaths, 2025. Available from: `https://data.who.int/dashboards/covid19/deaths`.
2. C. T. Bauch, A. d'Onofrio, P. Manfredi, Behavioral epidemiology of infectious diseases: An overview, in *Modeling the interplay between human behavior and the spread of infectious diseases*, Springer, New York, 2013, 1–19. https://doi.org/10.1007/978-1-4614-5474-8_1
3. T. Oraby, V. Thampi, C. T. Bauch, The influence of social norms on the dynamics of vaccinating behaviour for paediatric infectious diseases, *Proc. R. Soc. B*, **281** (2014), 20133172. https://doi.org/10.1098/rspb.2013.3172
4. S. Funk, M. Salathé, V. A. A. Jansen, Modelling the influence of human behaviour on the spread of infectious diseases: a review, *J. R. Soc. Interface*, **7** (2010), 1247–1256. https://doi.org/10.1098/rsif.2010.0142
5. C. T. Bauch, A. P. Galvani, Social factors in epidemiology, *Science*, **342** (2013), 47–49. https://doi.org/10.1126/science.1244492
6. Y. Ibuka, M. Li, J. Vietri, G. B. Chapman, A. P. Galvani, Free-riding behavior in vaccination decisions: an experimental study, *PLoS ONE*, **9** (2014), e87164. https://doi.org/10.1371/journal.pone.0087164
7. C. E. Wagner, J. A. Prentice, C. M. Saad-Roy, L. Yang, B. T. Grenfell, S. A. Levin, et al., Economic and behavioral influencers of vaccination and antimicrobial use, *Front. Public Health*, **8** (2020), 614113. https://doi.org/10.3389/fpubh.2020.614113
8. D. A. Henderson, P. Klepac, Lessons from the eradication of smallpox: An interview with D. A. Henderson, *Phil. Trans. R. Soc. B*, **368** (2013), 20130113. https://doi.org/10.1098/rstb.2013.0113
9. H. Heesterbeek, R. M. Anderson, V. Andreasen, S. Bansal, D. D. Angelis, C. Dye, et al., Modeling infectious disease dynamics in the complex landscape of global health, *Science*, **347** (2015), aaa4339. https://doi.org/10.1126/science.aaa4339
10. Z. Wang, C. T. Bauch, S. Bhattacharyya, A. d'Onofrio, P. Manfredi, M. Perc, et al., Statistical physics of vaccination, *Phys. Rep.*, **664** (2016), 1–113. https://doi.org/10.1016/j.physrep.2016.10.006
11. C. T. Bauch, D. J. D. Earn, Vaccination and the theory of games, *Proc. Natl. Acad. Sci. USA*, **101** (2004), 13391–13394. https://doi.org/10.1073/pnas.0403823101
12. T. C. Reluga, C. T. Bauch, A. P. Galvani, Evolving public perceptions and stability in vaccine uptake, *Math. Biosci.*, **204** (2006), 185–198. https://doi.org/10.1016/j.mbs.2006.08.015
13. F. Xu, R. Cressman, Disease control through voluntary vaccination decisions based on the smoothed best response, *Comput. Math. Methods Med.*, **2014** (2014), 825734. https://doi.org/10.1155/2014/825734

14. F. A. C. C. Chalub, P. Doutor, P. Patrício, M. C. Soares, Social vs. individual age-dependent costs of imperfect vaccination, *Math. Biosci.*, **375** (2024), 109259. https://doi.org/10.1016/j.mbs.2024.109259

15. C. T. Bauch, Imitation dynamics predict vaccinating behaviour, *Proc. R. Soc. B*, **272** (2005), 1669–1675. https://doi.org/10.1098/rspb.2005.3153

16. C. T. Bauch, S. Bhattacharyya, Evolutionary game theory and social learning can determine how vaccine scares unfold, *PLoS Comput. Biol.*, **8** (2012), e1002452. https://doi.org/10.1371/journal.pcbi.1002452

17. A. d'Onofrio, P. Manfredi, P. Poletti, The impact of vaccine side effects on the natural history of immunization programmes: an imitation-game approach, *J. Theor. Biol.*, **273** (2011), 63–71. https://doi.org/10.1016/j.jtbi.2010.12.029

18. X. Feng, B. Wu, L. Wang, Voluntary vaccination dilemma with evolving psychological perceptions, *J. Theor. Biol.*, **439** (2018), 65–75. https://doi.org/10.1016/j.jtbi.2017.11.011

19. M. Z. Ndii, N. Anggriani, A. K. Supriatna, Imitation game dynamics of vaccine-decision making behaviour on dengue transmission dynamics, *AIP Conf. Proc.*, **2084** (2019), 020019. https://doi.org/10.1063/1.5094278

20. S. Bhattacharyya, C. T. Bauch, A game dynamic model for delayer strategies in vaccinating behaviour for pediatric infectious diseases, *J. Theor. Biol.*, **267** (2010), 276–282. https://doi.org/10.1016/j.jtbi.2010.09.005

21. B. Buonomo, R. Della Marca, A. d'Onofrio, M. Groppi, A behavioural modelling approach to assess the impact of COVID-19 vaccine hesitancy, *J. Theor. Biol.*, **534** (2022), 110973. https://doi.org/10.1016/j.jtbi.2021.110973

22. J. Hofbauer, K. Sigmund, *Evolutionary games and population dynamics*, Cambridge University Press, Cambridge, 1998. https://doi.org/10.1017/CBO9781139173179

23. A. d'Onofrio, P. Manfredi, P. Poletti, The interplay of public intervention and private choices in determining the outcome of vaccination programmes, *PLoS ONE*, **7** (2012), e45653. https://doi.org/10.1371/journal.pone.0045653

24. M. L. Taylor, T. W. Carr, An SIR epidemic model with partial temporary immunity modeled with delay, *J. Math. Biol.*, **59** (2009), 841–880. https://doi.org/10.1007/s00285-009-0256-9

25. X. Chen, F. Fu, Imperfect vaccine and hysteresis, *Proc. R. Soc. B*, **286** (2019), 20182406. https://doi.org/10.1098/rspb.2018.2406

26. P. Doutor, R. Castelhano, M. C. Soares, B. V. Guerrero, N. Stollenwerk, M. Aguiar, et al., Complex dynamics in an epidemic model with imitation-driven vaccination strategy, *SIAM J. Appl. Dyn. Syst.*, **24** (2025), 1–34. https://doi.org/10.1137/24M1703707

27. M. G. M. Gomes, L. J. White, G. F. Medley, Infection, reinfection, and vaccination under suboptimal immune protection: Epidemiological perspectives, *J. Theor. Biol.*, **228** (2004), 539–549. https://doi.org/10.1016/j.jtbi.2004.02.017

28. R. Cressman, Y. Tao, The replicator equation and other game dynamics, *Proc. Natl. Acad. Sci. USA*, **111** (2014), 10810–10817. https://doi.org/10.1073/pnas.1400823111

29. M. Aguiar, S. Ballesteros, B. W. Kooi, N. Stollenwerk, The role of seasonality and import in a minimalistic multi-strain dengue model capturing differences between primary and secondary infections, *J. Theor. Biol.*, **289** (2011), 181–196. https://doi.org/10.1016/j.jtbi.2011.08.043

30. J. Duarte, C. Januário, N. Martins, S. Rogovchenko, Y. Rogovchenko, Chaos analysis and explicit series solutions to the seasonally forced SIR epidemic model, *J. Math. Biol.*, **78** (2019), 2235–2258. https://doi.org/10.1007/s00285-019-01342-7

31. N. Stollenwerk, S. Spaziani, J. Mar, I. E. Arrizabalaga, D. Knopoff, N. Cusimano, et al., Seasonally forced SIR systems applied to respiratory infectious diseases, bifurcations, and chaos, *Comput. Math. Methods Med.*, **2022** (2022), 3556043. https://doi.org/10.1155/2022/3556043

32. E. Gabrielli, Evaluate the Lyapunov spectrum of a dynamical system described by ODEs (in Python), GitHub repository, 2022. Available from: `https://github.com/dodogabrie/evaLEs`.

33. G. Benettin, L. Galgani, A. Giorgilli, J.-M. Strelcyn, Lyapunov characteristic exponents for smooth dynamical systems, *Meccanica*, **15** (1980), 21–30. https://doi.org/10.1007/BF02128237

34. T. C. Reluga, A. P. Galvani, A general approach for population games with application to vaccination, *Math. Biosci.*, **230** (2011), 67–78. https://doi.org/10.1016/j.mbs.2011.01.003

35. Y. A. Kuznetsov, *Elements of applied bifurcation theory*, Springer, New York, 2004. https://doi.org/10.1007/978-1-4757-3978-7

36. A. Dhooge, W. Govaerts, Y. A. Kuznetsov, New features of the software MatCont for bifurcation analysis of dynamical systems, *Math. Comput. Model. Dyn. Syst.*, **14** (2008), 147–175. https://doi.org/10.1080/13873950701742754

37. E. J. Doedel, B. Oldeman, AUTO-07p: Continuation and bifurcation software for ordinary differential equations, Concordia University, Montreal, 2012.

38. M. Aguiar, B. Kooi, N. Stollenwerk, Epidemiology of dengue fever: a model with temporary cross-immunity, *Math. Model. Nat. Phenom.*, **3** (2008), 48–70. https://doi.org/10.1051/mmnp:2008070

39. L. Yang, B. T. Grenfell, M. J. Mina, Waning immunity and re-emergence of measles and mumps in the vaccine era, *Curr. Opin. Virol.*, **40** (2020), 48–54. https://doi.org/10.1016/j.coviro.2020.05.009

40. J. Mossong, D. J. Nokes, W. J. Edmunds, M. J. Cox, S. Ratnam, C. P. Muller, Modeling the impact of subclinical measles transmission in vaccinated populations with waning immunity, *Am. J. Epidemiol.*, **150** (1999), 1238–1249. https://doi.org/10.1093/oxfordjournals.aje.a009951

41. J. Mossong, C. P. Muller, Modelling measles re-emergence as a result of waning of immunity in vaccinated populations, *Vaccine*, **21** (2003), 4597–4603. https://doi.org/10.1016/S0264-410X(03)00449-3

AIMS Press